Journal of Engineering Mathematics **38:** 355–370, 2000.

Potential flow past a sphere touching a tangent plane

SIMON J. COX* and MARK J. COOKER
*School of Mathematics, University of East Anglia, Norwich, NR4 7TJ, U.K.; *Present address: Department of Physics, Trinity College, Dublin 2, Ireland; E-mail: coxs@tcd.ie*

Received 13 January 1999; accepted in revised form 24 January 2000

Abstract. The uniform ideal flow past an impermeable sphere in contact with an impermeable plane is calculated, and the potential Φ is expressed as an integral over solutions in tangent sphere coordinates, up to an unknown function α. An ordinary differential equation satisfied by α is solved numerically to a high degree of accuracy and then a detailed presentation of the potential near the sphere is given. The potential near to the point of contact is analysed separately using a theory appropriate to crevice regions, and the two solutions are matched. The potential Φ is interpreted as the pressure impulse, P, for which the uniform gradient is specified far from the sphere. This provides information about the impulsive velocity and the net fluid impulse on the sphere or other blunt body near a region of wave impact. **Key words:** breaking waves, impulsive motion, potential flow, wave impact pressures

1. Introduction

We calculate the velocity potential Φ for uniform fluid flow past a sphere which is in contact with a flat plane. This is the simplest geometry in which to consider the more general problem of two bodies in point contact. Our interest arises from trying to model the fluid impulse on a body which is resting on an impermeable surface in the vicinity of a sea-wave impact. It may be that this wave-impact force will be great enough to overcome the natural forces which normally anchor such a body in place, which could help to explain how boulders are moved around on a beach during storms.

Shingle beaches are a prevalent feature of Britain's coastline. During storms, shingle is often washed onshore so that beaches are steeper in winter. In the summer the generally smaller waves draw shingle away from the beach to offshore bars. Wave action on beaches also tends to grade beach material, pushing larger particles farther up the beach (landward). When the beach material is a mixture of pebbles of different sizes, large particles move over the fine material and are thrown up on the shore [1]. We treat a blunt, randomly shaped boulder as a sphere which is subjected to an impulsive flow when a sea wave breaks nearby. The fluid impulse on the sphere is found from the pressure-impulse field, which is a potential, with boundary conditions which are the same as for uniform flow past a sphere touching a tangent plane. In this way, it can be demonstrated that large boulders will move farther up or down the beach than small boulders (see [2]).

When a wave of height h overturns and breaks against a sea wall, the fluid, of density ρ, undergoes a sudden change in its velocity field at every point. For laboratory waves, this change occurs over a timescale of the order of one millisecond. It is associated with a large brief acceleration, which is in turn associated with a large pressure gradient, directed away from the wall. This coincides with high values of pressure p, which have been reported by experimentalists since Bagnold [3]. Laboratory and field measurements [4, 5] show that the maximum pressures can be more than $10\rho gh$, ten times greater than the (mainly hydrostatic)

pressure exerted on the sea bed by non-breaking waves, where g is the acceleration due to gravity.

During the short time of impact the fluid acceleration and the pressure gradient balance in such a way that we may treat the change in the velocity field as occurring impulsively. We define the pressure impulse to be

$$P(x, y, z) = \int_{t_b}^{t_a} p(x, y, z, t)\, \mathrm{d}t, \tag{1}$$

where $[t_b, t_a]$ is the time interval of impact and x, y, z are coordinates in the fluid. Cooker and Peregrine [6] show that, provided the duration of impact, $t_a - t_b$, is short enough, we have approximately

$$\nabla P = \rho\,(\mathbf{u_b} - \mathbf{u_a})\,, \tag{2}$$

where $\mathbf{u_b}$ and $\mathbf{u_a}$ are the fluid velocities before and after impact, respectively. For a fluid which is incompressible before and after impact, P satisfies Laplace's equation

$$\nabla^2 P = 0, \tag{3}$$

even if the flow is rotational. Any vorticity in the flow is unchanged by the impulsive pressure because the curl of (2) implies that the change in vorticity is zero. Equation (3) must be solved subject to the boundary conditions (i) $\nabla P \cdot \mathbf{n} = 0$ on a fixed impermeable surface (with normal vector $\mathbf{n}$) which is in contact with the fluid before and after impact; (ii) $\nabla P \cdot \mathbf{n} = \rho \mathbf{u_b} \cdot \mathbf{n}$ where fluid impacts on a solid surface with velocity $\mathbf{u_b}$ and remains in contact with the surface after impact; (iii) P or ∇P specified in the far field; (iv) $P = 0$ on a free surface (since pressure, p, is constant on a free surface, we can define P up to an arbitrary constant, and without loss of generality this constant is zero).

Our interest is in the pressure impulse (and the underlying pressure) because we wish to calculate the impulse on a body which is either fixed or free to move and which lies in the region of a wave impact. Cooker and Peregrine [7] predict, and Grilli, Losada and Martin [8] have measured, the peak pressure field on the wall and bed of a wave tank in which wave impacts occur. Larger pressure impulses are found on the wall at the places where a wave impacts. The pressure impulse decreases towards zero with increasing distance from the site of impact. In particular there is a pressure-impulse gradient along, and parallel to, the bed. For a small enough body on the bed, this gradient can be modelled as a far-field boundary condition

$$-\nabla P \sim G\mathbf{i} \qquad \text{or} \qquad P \sim P_0 - Gx \tag{4}$$

as $r \to \infty$, where $\mathbf{i}$ is a unit vector in the x direction, along the bed away from the impact, r is radial distance from the centre of the body and $P_0 > 0$ and $G > 0$ are constants which depend upon the location of the body and the field of pressure impulse in the large-scale view. Cooker and Peregrine [7] consider simple bodies such as hemi-ellipsoids face-down on the bed, but we wish to extend the analysis to bodies in point contact. We solve Laplace's equation subject to (4) and $\partial P/\partial n = 0$ on the sphere and plane. If we suppose in (2) that $\mathbf{u_b} = 0$ and $\mathbf{u_a} = \nabla\Phi$ is the necessarily irrotational flow after an impulsive start, then we may take

$$P = -\rho\Phi.$$

We are then led to consider the artificial problem of the ideal flow past a sphere on a tangent plane, and can formulate the boundary-value problem for P in terms of the more familiar language of the velocity potential Φ. We reduce the flow at infinity to rest and consider the sphere to move with constant velocity $G/\rho\mathbf{i}$ parallel to and touching the plane. Φ is also the velocity potential for uniform flow perpendicular to the line joining the centres of two, equally sized, touching spheres.

This problem is harder than finding the potential around two touching spheres in axi-symmetric flow solved by Collins [9]. Lamb [10, Articles 80, 98, 99] uses an image system to construct a series solution for the potential for flows perpendicular to, or in line with, the centres of the spheres. His series are expansions in powers of non-zero gap width between the two spheres. These solutions converge too slowly to be accurate as the gap width tends to zero, although they are valid for separated spheres [11]. Li *et al.* [12] use spherical harmonics to show that the impermeability boundary condition is approximated with greatest error in the neighbourhood of the point of contact. Laplace's equation is solved by Solomentsov *et al.* [13] to find the conductivity around two touching spheres. They apply matched asymptotic expansions to the problem of a sphere separated by a small distance h from the plane and they show that, in the context of the hydrodynamic potential flow, as $h \to 0$ there is a singularity in the fluid velocity near the contact point. Latta and Hess [14] also tackle the small gap problem in the context of critical velocity phenomena in superfluid helium. They find the same singularity in the velocity at the contact point. Davis [15], whose work we most closely follow, considers two spheres heaving in phase on the surface of a liquid half-space. When the spheres touch, he is led to consider the present problem. The added mass coefficient for a sphere on a tangent plane, for movement parallel to the plane, is reported by Davis [15] to be 0·621 and we confirm this value.

The flow in the crevice near the point of contact can be approximated by averaging the potential over the small vertical distance between the plane and the lower surface of the sphere. This is presented in Section 2. The full three-dimensional potential problem is solved in Section 3. The solution is expressed as an integral over functions given by the solutions of Laplace's equation in tangent-sphere coordinates. The integral contains an unknown function $\alpha(q)$ which satisfies an ordinary differential equation. A highly accurate numerical solution for $\alpha(q)$ is found in Section 3.2 and compared with an asymptotic solution reported by Davis [15]. In Section 4.1 we discuss the numerical results for the potential around the sphere and compare them with the solution in the crack near the point of contact. The potential is continuous, but has a derivative singularity at the point of contact. The errors in the results are reported in Section 4.2 and shown to be much smaller than those for existing solutions of this problem. The benefit of calculating the pressure impulse P is that we can compute the added mass and the net impulse on the sphere. We do this for a fixed sphere with the fluid at infinity impelled according to (4) in Section 4.3. Then we modify the results to allow for the movement of a free sphere due to the fluid impulse, with the same far-field conditions.

2. Potential in the crack near the contact point

In the thin crevice near the point of contact between the sphere and its tangent plane, the velocity potential Φ satisfies Laplace's equation, $\nabla^2\Phi = 0$. The boundary conditions on both the sphere, S_1, and the plane, S_2, are

$$\nabla\Phi \cdot \mathbf{n}_\mathbf{i}|_{S_i} = 0, \qquad i = 1, 2, \tag{5}$$

where $\mathbf{n_i}$ denotes a normal to the surface S_i. If S_i is defined by the equation $z = f_i(x, y)$ then $\mathbf{n}_i = (-\partial f_i/\partial x, -\partial f_i/\partial y, 1)$ and (5) becomes

$$\left.\frac{\partial \Phi}{\partial z}\right|_{S_i} = \left.\frac{\partial \Phi}{\partial x}\right|_{S_i} \frac{\partial f_i}{\partial x} + \left.\frac{\partial \Phi}{\partial y}\right|_{S_i} \frac{\partial f_i}{\partial y}, \qquad i = 1, 2. \tag{6}$$

As in the derivation of shallow-water-wave theory (see, for example, [16]), we integrate Laplace's equation across the height of the crack and assume that the derivatives of each of the f_i are small. Then (6) implies that $\partial\Phi/\partial z$ is small on each of the bounding surfaces and therefore the x and y derivatives of Φ vary little across the gap and can be treated as independent of z. Defining $h(x, y) = f_2 - f_1 > 0$ we have the approximation

$$h\Phi_{xx} + h\Phi_{yy} + h_x\Phi_x + h_y\Phi_y = \nabla \cdot (h\nabla\Phi) = 0, \tag{7}$$

where now ∇ is the two-dimensional differential operator and x and y subscripts denote derivatives.

For a sphere of radius R, we employ plane polar coordinates (r, θ), where $r = 0$ is the point of contact, so that (7) is

$$\Phi_{rr} + \left(\frac{h_r}{h} + \frac{1}{r}\right)\Phi_r + \frac{\Phi_{\theta\theta}}{r^2} = 0, \tag{8}$$

and put $f_1 \equiv 0$ and $h(r) = f_2 = r^2/2R$. At the outer edge of the crack, as $r \to \infty$, we expect the solution to match that for a constant flow parallel to the x axis, for which $\Phi \propto \cos\theta$. A separable solution to (8), which is finite and integrable over the domain, is

$$\Phi_c(r, \theta) = Ar^{2^{1/2}-1}\cos\theta, \tag{9}$$

which is the required approximate solution for the potential, Φ_c, in the crack under the sphere (in agreement with the analysis of Solomentsov *et al.* [13]). The constant A will be chosen such that Φ_c matches a solution exterior to the crack at some appropriate value of r. Note that the velocity, $\mathbf{u} = \nabla\Phi_c$, is singular at the point of contact.

3. Fully three-dimensional flow past a sphere on its tangent plane

We now pose the problem as a sphere moving along its tangent plane with the fluid at rest at infinity. The instantaneous point of contact is at the origin and the tangent plane is the (x, y)-plane. The sphere moves at unit speed in the direction of the positive x axis ($G = |\mathbf{G}| = |\mathbf{i}| = 1$) and the z axis pierces the sphere along a diameter.

3.1. Formulation of the potential

We use tangent-sphere coordinates [17, p. 104]:

$$x = \frac{2\mu\cos\theta}{\mu^2 + \nu^2}, \quad y = \frac{2\mu\sin\theta}{\mu^2 + \nu^2}, \quad z = \frac{2\nu}{\mu^2 + \nu^2}$$

or

$$\mu = \frac{2(x^2 + y^2)^{1/2}}{x^2 + y^2 + z^2}, \quad \nu = \frac{2z}{x^2 + y^2 + z^2}, \quad \tan\theta = \left(\frac{y}{x}\right).$$

The origin corresponds to $\mu = \infty$ and $\mu = 0$ lies at infinity. Surfaces of constant μ are toroids without centre opening, and surfaces of constant ν are spheres tangent to the (x, y)-plane at the origin. The (x, y)-plane is defined by $\nu = 0$ and we choose the surface $\nu = 1$ to be our sphere, which has unit radius.

For any scalar function $\mathcal{E}$, Moon and Spencer [17] give

$$\nabla\mathcal{E} = \frac{\mu^2 + \nu^2}{2}\left(\frac{\partial\mathcal{E}}{\partial\mu}\hat{\boldsymbol{\mu}} + \frac{\partial\mathcal{E}}{\partial\nu}\hat{\mathbf{v}} + \frac{1}{\mu}\frac{\partial\mathcal{E}}{\partial\theta}\hat{\boldsymbol{\theta}}\right),$$

where $\hat{\boldsymbol{\mu}}$, $\hat{\mathbf{v}}$, $\hat{\boldsymbol{\theta}}$ are unit vectors normal to the level surfaces of μ, ν, θ. They also give solutions of Laplace's equation of the form

$$\bar{\Phi} = \left(\mu^2 + \nu^2\right)^{\frac{1}{2}} M(\mu)N(\nu)\Theta(\theta), \tag{10}$$

where $M(\mu) = A_1 J_p(\mu q) + B_1 J_{-p}(\mu q)$, $N(\nu) = A_2\cosh(\nu q) + B_2\sinh(\nu q)$, $\Theta(\theta) = A_3\cos(p\theta) + B_3\sin(p\theta)$ and p is an integer. The boundary condition on the moving sphere $\nu = 1$ is

$$\left.\frac{\partial\Phi}{\partial n}\right|_{\nu=1} = -\nabla(x).\mathbf{n} = -\nabla(x).\hat{\mathbf{v}} = -\frac{\mu^2+1}{2}\left.\frac{\partial x}{\partial\nu}\right|_{\nu=1} = \frac{2\mu\cos\theta}{\left(\mu^2+1\right)}$$

and since

$$\frac{\partial n}{\partial\nu} = \frac{2}{\mu^2+\nu^2},$$

we have

$$\left.\frac{\partial\Phi}{\partial\nu}\right|_{\nu=1} = \left.\frac{\partial\Phi}{\partial n}\right|_{\nu=1}\frac{\partial n}{\partial\nu} = \frac{4\mu\cos\theta}{\left(\mu^2+1\right)^2}. \tag{11}$$

The velocity component normal to the plane is zero, so

$$\left.\frac{\partial\Phi}{\partial\nu}\right|_{\nu=0} = 0\,. \tag{12}$$

Finally, we require no singularity in Φ. The $\cos\theta$ dependence in (11) gives $p = 1$ (that is, Φ is everywhere proportional to $\cos\theta$ as for the approximate solution) and this, with (12), gives us that Φ must be of the form

$$\bar{\Phi} = C(q)(\mu^2+\nu^2)^{\frac{1}{2}}J_1(\mu q)\cosh(\nu q)\cos\theta.$$

Since q is a free parameter, we integrate $\bar{\Phi}$ over all positive q to obtain the following expression for the potential Φ:

$$\Phi(\mu, \nu, \theta) = (\mu^2+\nu^2)^{\frac{1}{2}}\cos\theta\int_0^\infty C(q)J_1(\mu q)\cosh(\nu q)\,\mathrm{d}q. \tag{13}$$

To find $C(q)$ the boundary condition (11) is applied to (13),

$$\begin{aligned}&(\mu^2+1)^{\frac{1}{2}}\cos\theta\int_0^\infty C(q)J_1(\mu q)q\ \sinh(q)\,\mathrm{d}q\\ &+(\mu^2+1)^{-\frac{1}{2}}\cos\theta\int_0^\infty C(q)J_1(\mu q)\cosh(\nu q)\,\mathrm{d}q = \frac{4\mu\cos\theta}{\left(\mu^2+1\right)^2}.\end{aligned}$$

Thus

$$\int_0^\infty C(q)J_1(\mu q)q\sinh(q)\left(\mu^2+1+\frac{\coth(q)}{q}\right)\mathrm{d}q=\frac{4\mu}{\left(\mu^2+1\right)^{3/2}}.$$

Let $\alpha(q)=C(q)q\sinh(q)$ then

$$\int_0^\infty \alpha(q)J_1(\mu q)\left(\mu^2+1+\frac{\coth(q)}{q}\right)\mathrm{d}q=\frac{4\mu}{\left(\mu^2+1\right)^{3/2}} \tag{14}$$

and (13) becomes

$$\Phi(\mu,\nu,\theta)=(\mu^2+\nu^2)^{\frac{1}{2}}\cos\theta\int_0^\infty \alpha(q)J_1(\mu q)\frac{\cosh(\nu q)}{q\sinh(q)}\mathrm{d}q. \tag{15}$$

3.2. Solution for $\alpha(q)$

Following Davis [15], the transform in (14) can be inverted by applying the operator

$$\mathcal{L}=\frac{\mathrm{d}}{\mathrm{d}q}\left[q\frac{\mathrm{d}}{\mathrm{d}q}\right]-\frac{1}{q}$$

and using the result

$$\int_0^\infty J_1(\mu q)q\ \mathrm{e}^{-q}\ \mathrm{d}q=\mu(\mu^2+1)^{-3/2}.$$

Then $\alpha(q)$ can be shown to satisfy

$$\frac{\mathrm{d}^2\alpha}{\mathrm{d}q^2}-\frac{1}{q}\frac{\mathrm{d}\alpha}{\mathrm{d}q}-\left(1+\frac{\coth(q)}{q}\right)\alpha=-4q\mathrm{e}^{-q}. \tag{16}$$

In order that the integral in (15) converges, the boundary conditions on (16) are $\alpha(0)=0$ and as $q\to\infty,\alpha(q)\to 0$. We solve (16) by writing it as a system of two first-order ordinary differential equations and then using an Euler shooting method with constant step size h; see Figure 1. The scheme requires that $\alpha'(0)$ be specified, which depends critically upon the step size. When h is decreased, the estimate for $\alpha'(0)$ must be decreased also. Any error in $\alpha'(0)$ leads to solutions which diverge as $q\to\infty$; the value of $\alpha'(0)$ which gives $\alpha\to 0$ as $q\to\infty$ is therefore unique. An initial guess for $\alpha'(0)$ is refined by trial and error, any inaccuracy showing itself in the divergence to $\pm\infty$ beyond some large value of q. ($h=1{\cdot}0\times10^{-5}$ provided acceptable accuracy, for which $\alpha'(0)=0{\cdot}05665416796618627178$.)

Once $\alpha(q)$ has been found, Φ is calculated by numerical integration of (15). This was carried out by means of a simple trapezoidal rule with intervals of width $h=2\times10^{-6}$ and the upper limit was truncated at $q=20{\cdot}0$. Davis found that for large q, $\alpha(q)\approx q^2\mathrm{e}^{-q}$ and in Figure 1 we see that this is a good approximation for all q. When μ and ν are small (corresponding to points in the fluid far from the sphere) the greatest contribution to the integral in (15) comes from large q. So replacing the numerically computed $\alpha(q)$ with $\bar{\alpha}(q)=q^2\mathrm{e}^{-q}$ led to similar values of Φ (compare Figures 6 and 8).

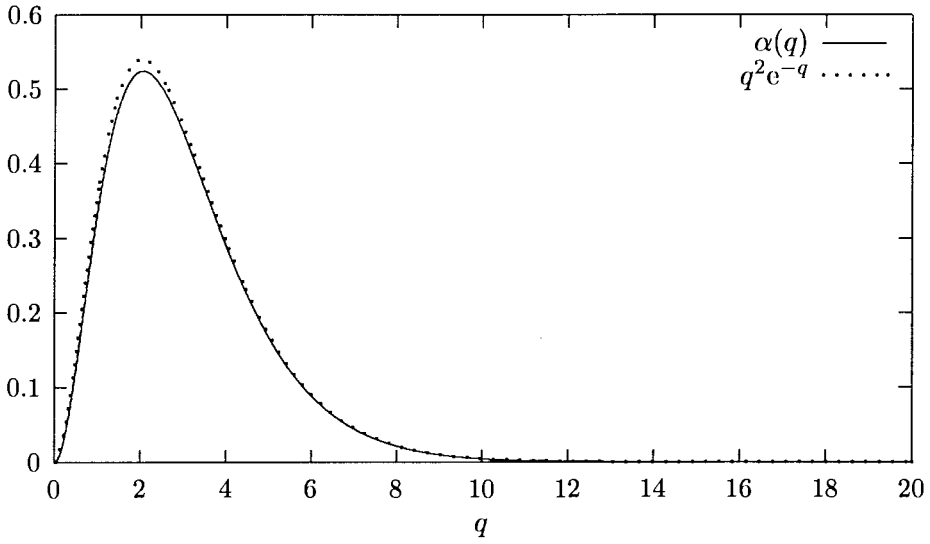

Figure 1. $\alpha(q)$, the solution of (14), compared with q^2e^{-q}. An Euler scheme was used, with step size $h = 1 \times 10^{-5}$ and $\alpha'(0) = 0{\cdot}05665416796618627178$.

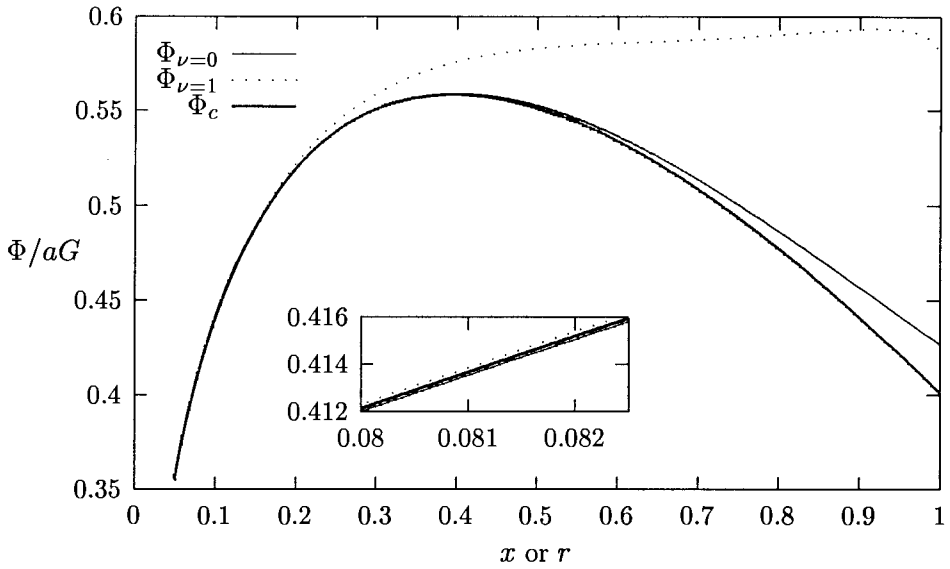

Figure 2. Comparison between the crack solution and three-dimensional theory in the plane $\theta = 0°$. Φ on the tangent plane and on the sphere bracket the crack solution $\Phi_c = 1{\cdot}401r^{2^{1/2}-1} - r$ for $r \leq 0{\cdot}4$. For larger values of r, $\Phi_c < \Phi$ on both the sphere and the plane. However, for $r < 0{\cdot}05$ we expect the crack solution to become even more accurate.

4. Results

4.1. Potential around the sphere

For a sphere moving along the x axis at unit speed, the crack solution (9) becomes

$$\Phi_c(r, \theta) = \left(Ar^{2^{1/2}-1} - r\right)\cos\theta. \tag{17}$$

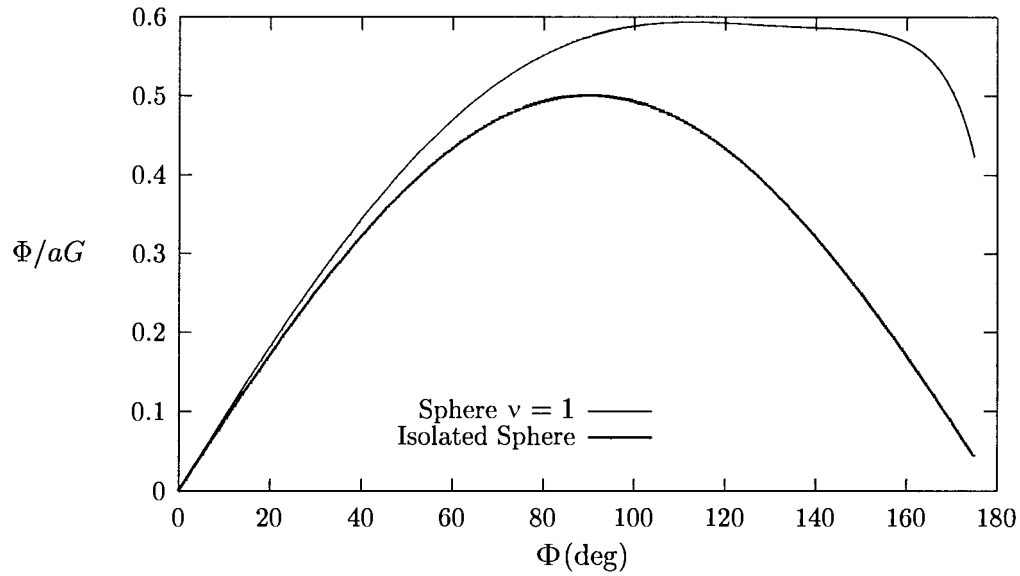

Figure 3. Φ as a function of angle ϕ on the sphere's surface, $\nu = 1$, and for an isolated sphere of unit radius ($\frac{1}{2}\sin\phi$). $\phi = 180°$ is the contact point. The maximum of Φ is $0{\cdot}594aG$ and occurs at $\phi = 112{\cdot}6°$. We see that the influence of the tangent plane is negligible near $\phi = 0°$.

We choose A so that Φ_c agrees best with Φ from the three-dimensional analysis of Section 3. At $r = 0{\cdot}05$ (one-twentieth of the sphere's radius) we constrain Φ_c to equal Φ, as found from the numerical evaluation of (15), on the sphere $\nu = 1$. This gives $A = 1{\cdot}401$ (applying the constraint at some $0{\cdot}02 \leq r \leq 0{\cdot}1$, we find $1{\cdot}401 \leq A \leq 1{\cdot}402$), which is comparable to $A = 1{\cdot}41$ estimated by Solomentsov *et al.* [13, Equation (47)] who use different criteria. This choice for Φ_c agrees well with Φ on the tangent plane for a wide interval of values of r as shown in Figure 2. Notice that, when $r \leq 0{\cdot}4$, the crack solution (17) lies between the curves for Φ on the plane ($\nu = 0$) and the sphere ($\nu = 1$) obtained from the fully three-dimensional solution. For slightly larger r the two-dimensional approximation becomes inadequate, this being the region where three-dimensional effects are significant. However, Φ_c is an excellent approximation beyond the range of r for which we would expect the theory to be valid. In Appendix A we show that the potential Φ has the same dependence on r as Φ_c, close to the contact point.

Elsewhere, the maximum value of Φ occurs on the lower part of the sphere at $\phi = 112{\cdot}6°$, as shown in Figure 3, where ϕ is the angle subtended at the sphere centre from the positive z axis. This maximum coincides with the stagnation point, which can be verified graphically from a plot of $\partial\Phi/\partial\mu$ against ϕ. Therefore the presence of the tangent plane moves the stagnation point $22{\cdot}6°$ towards the plane.

Figures 4–9 show isopotentials on two-dimensional sections near the sphere. On a plane of constant z, the transformation $x \to -x$ sends $\Phi \to -\Phi$ and $y \to -y$ sends $\Phi \to \Phi$. Similar symmetries apply for planes of constant y or x and therefore only a quarter of the domain is drawn.

For a sphere moving from left to right at unit speed, Figure 4 gives contours of constant Φ on the plane $z = \nu = 0{\cdot}0$. The bunching of contours near the origin corresponds to large flow speed around the point of contact. At the top of the sphere, on the plane $z = 2{\cdot}0$, Figure 5 shows the isopotentials. Figure 6 presents contours on a plane through the centre of the sphere,

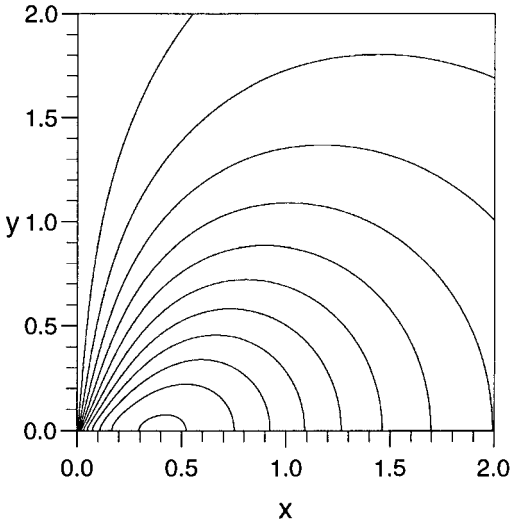

Figure 4. Isopotentials, from (15), on the tangent plane $z = v = 0{\cdot}0$. $\Phi = 0{\cdot}0$ on the y axis, contour separation $= 0{\cdot}05aG$. The sphere moves from left to right at unit speed.

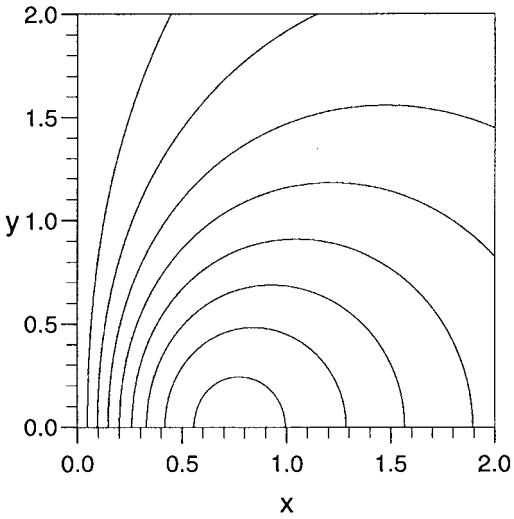

Figure 5. Isopotentials, from (15), on the top plane $z = 2{\cdot}0$. $\Phi = 0{\cdot}0$ on the y axis, contour separation $= 0{\cdot}025aG$. The sphere moves from left to right at unit speed.

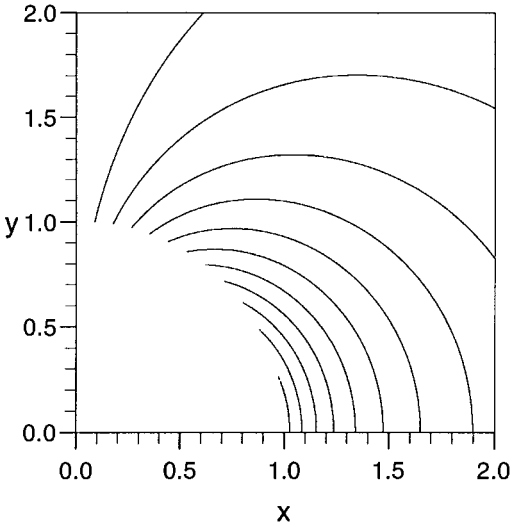

Figure 6. Isopotentials, from (15), on the equatorial plane $z = 1{\cdot}0$. $\Phi = 0{\cdot}0$ on the y axis, contour separation $= 0{\cdot}05aG$. The sphere moves from left to right at unit speed. Compare with Φ for an isolated sphere in Figure 4.1, and also with Figure 8.

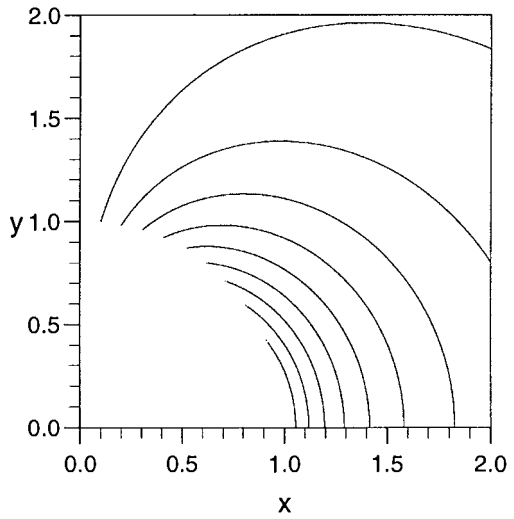

Figure 7. Isopotentials on the equatorial plane for an isolated sphere of unit radius. $\Phi = 0{\cdot}0$ on the y axis, contour separation $= 0{\cdot}05aG$. The sphere moves from left to right at unit speed.

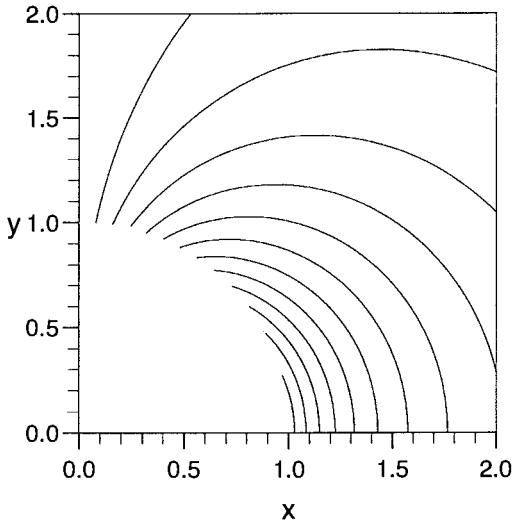

Figure 8. Isopotentials on the equatorial plane $z = 1{\cdot}0$, using the approximation $\alpha(q) = q^2 e^{-q}$ to evaluate (15). $\Phi = 0{\cdot}0$ on the y axis, contour separation $= 0{\cdot}05aG$. The sphere moves from left to right at unit speed. Compare with Figure 4.1.

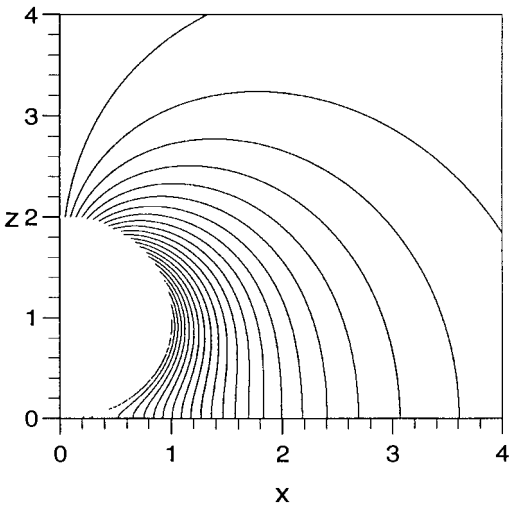

Figure 9. Isopotentials on the vertical plane $y = 0{\cdot}0$. $\Phi = 0{\cdot}0$ on the z axis, contour separation $= 0{\cdot}025aG$. The sphere moves from left to right at unit speed.

$z = 2{\cdot}0$ (which can be compared with the contours around an isolated sphere shown in Figure 7). Figure 8 also shows contours on $z = 1{\cdot}0$, but now the analytical approximation $\alpha(q) = q^2 e^{-q}$ has been used to evaluate Φ. The contours are nearly the same as in Figure 6; this shows the value of the approximation to $\alpha(q)$. In Figure 9 the isopotentials for the vertical plane $y = 0{\cdot}0$ are tightly bunched, indicating high fluid speeds.

If the sphere is held fixed, Figures 10 and 11 show how the presence of the sphere deforms uniform flow parallel to the x axis at unit speed, on the planes $z = 0{\cdot}0$ and $z = 1{\cdot}0$, respectively. The flow in Figure 11 is very similar to that for an isolated sphere, indicating that the influence of the tangent plane is small one radius away.

4.2. Errors in the numerical approximation

Figure 1 shows that $\alpha(q) \approx q^2 e^{-q}$, particularly for large q, which accords with Davis [15]. Very little improvement in the accuracy of $\alpha(q)$ is obtained by decreasing the step size; an Euler method with step size $h = 1 \times 10^{-5}$ is adequate. One measure of the error in our method is the difference between the calculated boundary condition on the sphere, $\partial\Phi/\partial\nu|_{\nu=1}(\mu)$, and the exact value of $4\mu/(\mu^2+1)^2$ on the plane $\theta = 0$. However, Li *et al.* [12] quantify their errors by examining the residual normal velocity component on the sphere, $v'(\phi)$. Here $v' = \frac{1}{2}(\mu^2+1)\,\partial\Phi/\partial\nu|_{\nu=1}(\mu)$ and therefore the error, E, is given by

$$E(\mu) = \frac{\mu^2+1}{2}\left[\left.\frac{\partial\Phi}{\partial\nu}\right|_{\nu=1} - \frac{4\mu}{(\mu^2+1)^2}\right]$$

as graphed in Figure 12. This is an improvement compared with the numerical error reported by Li *et al.* [12]. It is difficult to see how accurate their series representations of 1000

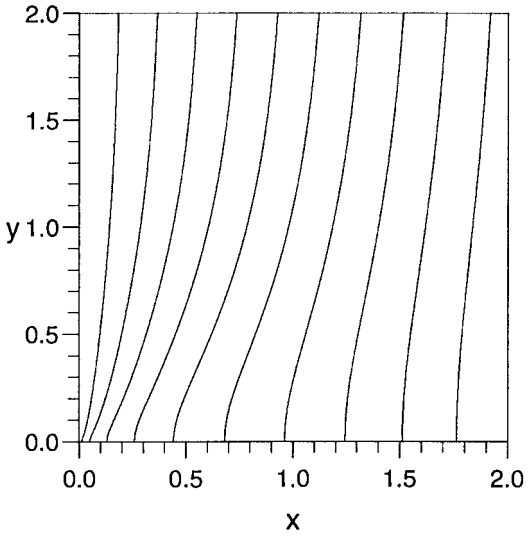

Figure 10. Isopotentials on the tangent plane $z = 0{\cdot}0$ for uniform flow from left to right past a stationary sphere. $\Phi = 0{\cdot}0$ on the y axis, contour separation $= 0{\cdot}2aG$. The point of contact is at the origin.

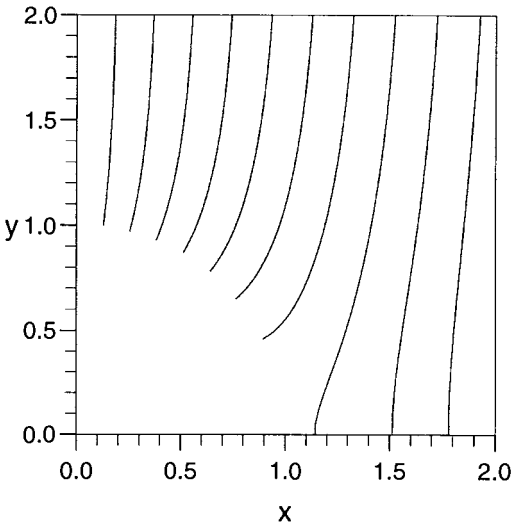

Figure 11. Isopotentials for uniform flow from left to right past a stationary sphere on the equatorial plane $z = 1{\cdot}0$. $\Phi = 0{\cdot}0$ on the y axis, contour separation $= 0{\cdot}1aG$. The isopotentials are very similar to those for an isolated sphere.

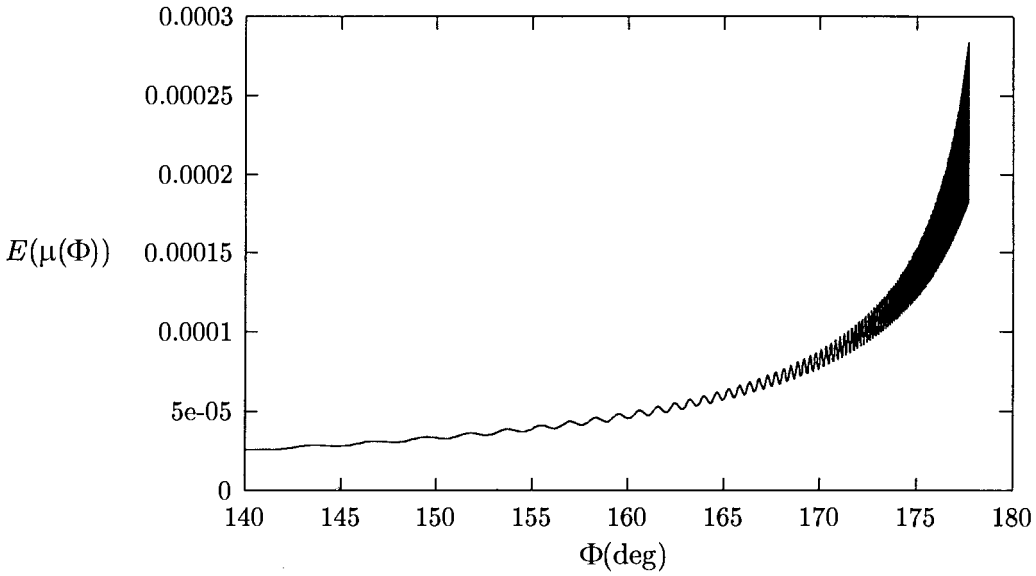

Figure 12. $E(\mu)$, the residual normal velocity component on the sphere, restricted to the plane $\theta = 0$. The step size is $h = 1 \times 10^{-5}$ and the integration for Φ is truncated at $q = 20$ (increasing this value of q, and using the analytical approximation $\bar{\alpha}(q)$ over the extended range, would decrease the error further). $\phi = 180^\circ$ is the contact point. At $\phi = 175^\circ$, $E = 0{\cdot}00015$. We follow Li *et al.* [12] in showing only $140^\circ \leq \phi \leq 180^\circ$.

terms are, especially since $\phi = 180°$ corresponds to $\mu = \infty$. However, it appears that our error at $\phi = 175°$ is 0·00015 compared to 0·01 for their results. We can further reduce the error in our method by using the analytical approximation $\bar{\alpha}(q)$ for $q > 20$. We remark that, if we made no allowance for the presence of the sphere, the residual normal velocity would be $G \sin\phi$, an error far in excess of that present here, except *very* close to the contact point. For $\phi > 175°$, which is equivalent to $r < 0{\cdot}043$, near to the point of contact, we can use the solution (9) with an error in Φ of less than 0·0001, as found by the proximity of the lines in an extension to Figure 2 for $r < 0{\cdot}05$.

4.3. Impulse and added mass

Cooker and Peregrine [7] suggest that the modulus of the impulse on a body depends upon its shape and volume. They report the impulse for a hemi-ellipsoid whose flat base rests on a flat bed, and a long circular log touching the bed. However, we wish to extend the calculations to more general three-dimensional bodies, particularly those that have a contact point. The simplest example of a body in point contact is a sphere on a horizontal plane.

We consider the pressure impulse $P = -\rho\Phi$, where Φ is computed from (15) for a moving sphere. We calculate the impulse, I_x, on the stationary sphere due to an impulsive flow of unit speed in the x direction at infinity. The pressure impulse for a stationary sphere is $-\rho\Phi + x$. Using spherical polar coordinates $(r = 1, \theta, \phi)$, with origin at the centre of the sphere, we obtain

$$\begin{aligned} I_x &= \int_0^{2\pi}\int_0^{\pi} (P(\theta,\phi) + x)|_{v=1} \ \cos\theta \sin\phi \ \sin\phi \, \mathrm{d}\phi \, \mathrm{d}\theta \\ &= \pi \int_0^{\pi} P|_{v=1}\,(\theta = 0, \phi) \sin^2\phi \, \mathrm{d}\phi + \frac{4\pi}{3}. \end{aligned} \tag{18}$$

Since

$$\cos\phi = \frac{1-\mu^2}{1+\mu^2}, \ \ \sin\phi = \frac{2\mu}{1+\mu^2} \text{ and } \sin\phi \, \mathrm{d}\phi = \frac{4\mu}{\left(1+\mu^2\right)^2} \, \mathrm{d}\mu,$$

we have

$$\begin{aligned} I_x &= 8\pi \int_0^{\infty} \frac{\mu^2}{\left(1+\mu^2\right)^3} P(\theta = 0, \mu)|_{v=1} \, \mathrm{d}\mu + \frac{4\pi}{3} \\ &= 8\pi \int_0^{\infty} \frac{\mu^2}{\left(1+\mu^2\right)^{5/2}} \int_0^{\infty} \frac{\coth(q) J_1(\mu q)\, \alpha(q)}{q} \, \mathrm{d}q \, \mathrm{d}\mu + \frac{4\pi}{3}. \end{aligned}$$

We performed the integration numerically, truncating at $\mu = 50$ (equivalent to $\phi = 177{\cdot}7°$) and $q = 50$, but using the approximation $\alpha(q) = q^2 \mathrm{e}^{-q}$ for $q > 8$. Then $I_x = 0{\cdot}828\pi + 4\pi/3 = 6{\cdot}790$. Writing $I_x = KV$, where $V = \frac{4}{3}\pi$ is the volume of the sphere, we have $K = 1{\cdot}621$. The added-mass coefficient $K - 1 = 0{\cdot}621$ which confirms the result of Davis [15]. Thus, for a sphere of radius a the added mass is $0{\cdot}621 \left(\frac{4}{3}\pi\rho a^3\right)$, which should be compared with $\frac{1}{2}\left(\frac{4}{3}\pi\rho a^3\right)$ for an isolated sphere.

If we denote by $s = \pi - \phi$ the arc length around the sphere from the contact point, then the contribution to the impulse I_x found above from the neighbourhood of the crack

$175^\circ = 3{\cdot}054^{\text{rad}} = \phi_0 \le \phi \le \pi^{\text{rad}} = 180^\circ$ is

$$\begin{aligned} I'_x &= \int_0^{2\pi} \int_{\phi_0}^{\pi} 1{\cdot}401 s^{2^{1/2}-1} \cos\theta . \cos\theta \sin\phi . \sin\phi \, \mathrm{d}\phi \, \mathrm{d}\theta \\ &= 1{\cdot}401\pi \int_0^{\pi-\phi_0} s^{2^{1/2}-1} \sin^2 s \, \mathrm{d}s \\ &= 1{\cdot}401\pi .7{\cdot}077 \times 10^{-5} = 3{\cdot}115 \times 10^{-4}, \end{aligned}$$

showing that the contribution to the total impulse from the area around the crack is in the next significant figure after $I_x = 6{\cdot}790$. From arguments based on symmetry, the components of the impulse in the y and z directions are zero: $I_y = I_z = 0$. So a horizontal gradient of pressure impulse, $G\mathbf{i}$, specified at infinity, gives a fixed sphere an impulse which is in the $\mathbf{i}$ direction. $\mathbf{I} = |I_x|\mathbf{i} = 1{\cdot}621 \left(\frac{4}{3}\pi a^3\right) \mathbf{G}$ is only 8% larger than the impulse experienced by an isolated sphere, $1{\cdot}5 \left(\frac{4}{3}\pi a^3\right) \mathbf{G}$. This small difference suggests that we can well-approximate the impulse on a blunt randomly shaped body by treating a sphere of the same volume. Since the impulse vector is parallel to $\mathbf{G}$ and to the plane, this work may help to explain the sudden movement of bodies away from a wave impact on a shingle beach. The pressure impulse gradient points up the beach above the wave impact and points down the beach below. Each pebble responds to the local applied pressure gradient; if it is free to move it acquires some initial speed from the fluid impulse and is eventually brought to rest by friction with neighbouring bodies, gravity and fluid resistance. In this way a body is displaced a short distance by each wave impact. A succession of impacts in one place can lead to the movement by many small steps of beach material both up and down the beach away from the site of impact.

We now suppose that the sphere has density ρ_b and is free to move. The fluid impulse generated by the pressure impulse gradient $G\mathbf{i}$ accelerates it from rest to a velocity $U\mathbf{i}$. We dimensionalise P from (18) and follow Cooker and Peregrine [7] in equating the change of momentum of the sphere, $\frac{4}{3}\pi\rho_b a^3 U$, with the impulse on it,

$$I_x = 0{\cdot}828\pi(G - \rho U)a^3 + \frac{4}{3}\pi a^3 G = \frac{4}{3}\pi a^3 \left(1{\cdot}621G - 0{\cdot}621\rho U\right).$$

Then the speed of the sphere is

$$U = \frac{1{\cdot}621G}{0{\cdot}621\rho + \rho_b} \tag{19}$$

and

$$I_x = \frac{4}{3}\pi a^3 G \frac{1{\cdot}621\rho_b}{0{\cdot}621\rho + \rho_b}. \tag{20}$$

For a sudden change of fluid speed of 10 m/s in water of density $\rho = 1000$ kg/m^3 we expect $G = 10^4$ kg/m^2/s. If the body has density $\rho_b = 3\rho$, then (19) gives an acquired speed (whatever its size) of $U \approx 4{\cdot}5$ m/s. This is almost one half of the fluid's speed, but we would expect the body to be rapidly brought to rest by frictional forces.

5. Conclusions

The calculations outlined above provide a method for determining and visualising the flow around a sphere on a tangent plane. The problem can be viewed as a stationary sphere at the

origin, with $\nabla\Phi$ a specified constant at infinity, or as a sphere moving in the direction of the positive x axis in fluid at rest at infinity. The errors, as measured by how closely the boundary condition on the sphere is satisfied, are significantly smaller than those of Li *et al.* [12].

Φ is the potential for ideal flow around a sphere on a tangent plane. It is directly proportional to the pressure impulse, P, a concept useful in coastal-wave impact. We envisage that this information will be useful in calculating the effects of wave impact on bodies such as roughly spherical boulders. In particular, the approximation in the crack (9) can be applied to a wider class of body in point contact with a plane, such as ellipsoids with small eccentricities, for which the potential retains the form $\Phi \propto r^{2^{1/2}-1}\cos\theta$ around the point of contact (see [18]). As with the sphere, this solution is valid over a wide region near the point of contact. However these bodies need full calculations to find the potential everywhere.

The sphere experiences no impulsive lift. The impulse is parallel to the applied pressure gradient **G** which is parallel to the tangent plane. For a fixed sphere of radius a the impulse is $\mathbf{I} = 1{\cdot}621\left(\frac{4}{3}\pi a^3\right)\mathbf{G}$.

Acknowledgements

The authors thank Prof. W.D. Collins and Prof. A.M.J. Davis for their helpful comments. SJC was supported by the UK Engineering and Physical Sciences Research Council, award number 96000215.

Appendix A. The behaviour of Φ at the point of contact

In order to discover more about how the velocity potential behaves near the contact point, we consider $\alpha(q)$ as $q \to 0$. Equation (16) is rewritten for small q as

$$\frac{\mathrm{d}^2\alpha}{\mathrm{d}q^2} - \frac{1}{q}\frac{\mathrm{d}\alpha}{\mathrm{d}q} - \frac{1}{q^2}\alpha \approx -4q$$

which has solution

$$\alpha(q) = -2q^3 + Aq^{2^{1/2}+1} + Bq^{1-2^{1/2}}, \tag{A1}$$

where A and B are constants. To exclude the singularity at $q = 0$ we put $B = 0$ and then consider (15). Near to the contact point, on the plane $z = \nu = 0$, we have $\mu = 2/r$, where r is the plane polar coordinate distance from the point of contact. Then the dominant contribution to

$$\Phi|_{\nu=0} = \mu\cos\theta\int_0^\infty \alpha(q)\frac{J_1(\mu q)}{q\sinh(q)}\mathrm{d}q$$

comes from $q \in [0, j/\mu]$, for some real number j, as $\mu \to \infty$. Making the substitution $q = t/\mu$, using (A1) for small q, and using $\alpha(q) = q^2\mathrm{e}^{-q}$ for large q we have

$$\Phi|_{\nu=0} = \mu\cos\theta\left\{\int_0^j\left(A\frac{t^{2^{1/2}-1}}{\mu^{2^{1/2}}} - \frac{2t}{\mu^2}\right)J_1(t)\mathrm{d}t + \int_{j/\mu}^\infty \frac{q\ \mathrm{e}^{-q}J_1(\mu q)}{\sinh(q)}\mathrm{d}q\right\}. \tag{A2}$$

We rewrite the second integral as

$$\begin{aligned} I_2 &= \int_{j/\mu}^{\infty} 2q\,J_1(\mu q) \sum_{n=1}^{\infty} \mathrm{e}^{-2nq}\,\mathrm{d}q \\ &= \int_{j}^{\infty} \frac{2x}{\mu^2} J_1(x) \sum_{n=1}^{\infty} \mathrm{e}^{-2nx/\mu}\,\mathrm{d}x \\ &\approx \int_{j}^{\infty} \frac{2x}{\mu} J_1(x) \int_{1/\mu}^{\infty} \mathrm{e}^{-2yx}\,\mathrm{d}y\;\mathrm{d}x \quad \text{as } \mu \to \infty \\ &= \mu^{-1} \int_{j}^{\infty} J_1(x)\mathrm{e}^{-2x/\mu}\,\mathrm{d}x. \end{aligned}$$

We next integrate I_2 by parts:

$$I_2 = \mu^{-1}\left[J_0(j)\mathrm{e}^{-2j/\mu} - \frac{1}{2\mu}\int_{j}^{\infty} J_0(x)\mathrm{e}^{-2x/\mu}\,\mathrm{d}x \right]$$

and choose j as the *first* zero of J_0: $J_0(j) = 0$. Then note that we have

$$\int_{j}^{\infty} J_0(x)\mathrm{e}^{-2x/\mu}\,\mathrm{d}x \le \int_{0}^{\infty} J_0(x)\mathrm{e}^{-2x/\mu}\,\mathrm{d}x = \left(1 + \frac{4}{\mu^2}\right) \approx 1$$

for large μ, using [19, Equation 6.611.1]. Thus I_2 is of order μ^{-2} at most and (A2) becomes

$$\begin{aligned} \Phi|_{v=0} &= \mu\cos\theta \left\{ \frac{A}{\mu^{2^{1/2}}} \int_0^1 t^{2^{1/2}-1} J_1(t)\,\mathrm{d}t - \frac{2}{\mu^2}\int_0^1 t\,J_1(t)\,\mathrm{d}t + O(\mu^{-2}) \right\} \\ &\approx \cos\theta \left\{ A'\mu^{1-2^{1/2}} + O(\mu^{-1}) \right\} \\ &= \cos\theta \left\{ A''r^{2^{1/2}-1} + O(r) \right\} \end{aligned}$$

which is immediately comparable with the expression (17) for Φ_c, showing that the fully three-dimensional solution has the same dependence on r close to the origin.

References

1. V.P. Zenkovich, *Processes of Coastal Development.* London: Oliver & Boyd (1967) 738 pp.
2. S.J. Cox and M.J. Cooker, The Motion of a Rigid Body Impelled by Sea-Wave Impact. *Appl. Ocean Res.* 21 (1999) 113–125.
3. R.A. Bagnold, Beach Formation by Waves; Some Model-Experiments in a Wave Tank. *J. Inst. Civil Eng.* 12 (1939) 201–226.
4. P.A. Blackmore and P.J. Hewson, Experiments on full-scale wave impact pressures. *Coastal Eng.* 8 (1984) 331–346.
5. E.S. Chan and W.K. Melville, Deep-water plunging wave pressures on a vertical plane wall. *Proc. R. Soc. London* A 417 (1988) 95–131.
6. M.J. Cooker and D.H. Peregrine, Pressure-impulse theory for liquid impact problems. *J. Fluid Mech.* 297 (1995) 193–214.
7. M.J. Cooker and D.H. Peregrine, Wave impact pressure and its effect upon bodies lying on the sea bed. *Coastal Eng.* 18 (1992) 205–229.
8. S.T. Grilli, M.A. Losada and F. Martin, Wave Impact Forces on Mixed Breakwaters *Proc. 23rd Intl. Conf. Coastal Eng.*, ASCE, Venice, Italy (1993) 1161–1174.

9. W.D. Collins, On the solution of some axisymmetric boundary value problems by means of integral equations III. Some electrostatic and hydrodynamic problems for two spherical caps. *Proc. London Math. Soc.* (3) 10 (1960) 428–460.
10. H. Lamb, *Hydrodynamics.* 6th edition. Cambridge : Cambridge University Press (1932) 738pp.
11. I. Eames, J.C.R. Hunt and S.E. Belcher, Displacement of inviscid fluid by a sphere moving away from a wall. *J. Fluid Mech.* 324 (1996) 333–353.
12. L. Li, W.W. Schultz and H. Merte, The velocity potential and the interacting force for two spheres moving perpendicularly to the line joining their centers. *J. Eng. Maths.* 27 (1993) 147–160.
13. Y. Solomentsev, D. Velegol and J.L. Anderson, Conduction in the small gap between two spheres. *Phys. Fluids* 9 (1997) 1209–1217.
14. G.E. Latta and G.B. Hess, Potential flow past a sphere tangent to a plane. *Phys. Fluids* 16 (1973) 974–976.
15. A.M.J. Davis, High frequency limiting virtual-mass coefficients of heaving half-immersed spheres. *J. Fluid Mech.* 80 (1977) 305–319.
16. J.J. Stoker, *Water Waves.* New York: Wiley (1992) 567 pp.
17. P. Moon and D.E. Spencer, *Field Theory Handbook.* Berlin: Springer (1961) 236 pp.
18. S.J. Cox, *Pressure Impulses caused by Wave Impact.* PhD Thesis: School of Mathematics, University of East Anglia (1998) 199 pp.
19. I.S. Gradshteyn and I.M. Ryzhik, *Table of Integrals, Series, and Products.* New York: Academic Press (1965) 1160 pp.